Iraqi Journal of Science, 2022, Vol. 63, No. 1, pp: 131-148
DOI: 10.24996/ijs.2022.63.1.15

ISSN: 0067-2904

Recent Development-2 of CADTEL Software: The Optimum Conditions of Scherzer Imaging in the Electron Magnetic Lenses

Hussain S. Hasan[1], Sura Allawi Obaid[1], Muhssen Salbookh Erhayief[2]
[1]*Department of Physiology and Medical Physics, College of Medicine, Al-Nahrain University, Baghdad, Iraq*
[2]*Department of Physics, College of Education, Mustansiriyah University, Baghdad, Iraq*

Received: 13/9/2020 Accepted: 10/3/2021

Abstract

CADTEL software was developed to provide the simplest and most versatile computing resource that a wide range of skilled researchers and designers can use. In this paper, a development on this program, relying on sixteen mathematical models, produced a new version of CADTEL software package which focuses on the optimum conditions of Scherzer imaging for round electron magnetic lenses.. These models depend on synthesis procedure which is mainly designed to work with the inverse design problem, and represent the axial magnetic flux density of desirable electron magnetic lens which can be proposed or selected , using the four (zero, low, high, infinite) magnification states. The program provides the freedom of selecting multiple models and changing its variables (which appear on the home page), in addition to providing facilities for numerous proposed magnetic lens. The objective properties calculated in the program were used to compute and plot the optimum conditions for Scherzer imaging

The CADTEL software was written in Visual Basic – 6, in an easy-to-use mode, even for a beginner computer user. The results of the analysis clearly show that there is an excellent equivalent calculation which could be obtained for the same lens from CADTEL software when evaluated with other counterpart software.

Keywords: Magnetic lens, Scherzer imaging, spherical aberration, resolution limit.

التطوير الحديث–2 لبرنامج CADTEL: الشروط المثلى لتصوير شيرزر للعدسات الكهرومغناطيسية

حسين صالح حسن[1] ، سرى علاوي عبيد[1] ، محسن صلبوخ ارهيف[2]
[1]فرع علم وظائف الاعضاء (الفسلجة)، كلية الطب، جامعة النهرين، بغداد، العراق
[2]قسم الفيزياء، كلية التربية، الجامعة المستنصرية، بغداد، العراق

الخلاصة

في السابق، تم تطوير برنامج CADTEL لتوفير أبسط موارد الحوسبة وأكثرها تنوعًا والتي يمكن لمجموعة واسعة من الباحثين والمصممين المهرة استخدامها. بينما، التطوير الحالي,المقدم في هذا البحث, هو نسخة جديدة من حزمة برامج CADTEL حيث الاهتمام بالشروط المثلى لتصوير شيرزر للعدسات المغناطيسية الإلكترونية المدورة، ضمن ستة عشر نموذجًا رياضيًا. تعتمد هذه النماذج على الطريقة التوليفية في التصميم بشكل أساسي للعمل مع مشكلة التصميم العكسي وتمثيل كثافة الفيض المغناطيسي المحوري للعدسة المغناطيسية الإلكترونية المرغوبة والتي يمكن اقتراحها أو اختيارها باستخدام حالات التكبير الأربعة (الصفري، الواطيء، العالي، و اللانهائي). البرنامج يوفر لنا حرية اختيار نماذج متعددة وتغيير معاملاتها (التي تظهر

*Email: altai1965@yahoo.com

في الصفحة الرئيسية للبرنامج) وتسهيلات للعديد من العدسات المغناطيسية المقترحة. تستخدم الخواص الشيئية المحسوبة في البرنامج لحساب ورسم الشروط المثلى لتصوير شيرزر.
تمت كتابة برنامج CADTEL في لغة فيجوال بيسك (Visual Basic – 6)، بشكل سهل الاستخدام حتى في حالة وان كان مستخدم الكمبيوتر مبتديء. تظهر نتائج التحليل بوضوح أن هناك تكافوء ممتاز يمكن الحصول عليه لنفس العدسة من برنامج CADTEL عند تقييمه باستخدام برنامج نظيرة آخرى.

1. Introduction

1.1 Background

The CADTEL software [1], is a package of programs in the field of design and simulation for charged particles optics, is to be develop in the current paper. Since the beginning of the second half of the last century, the idea of using a computer as a tool for analyzing electron lenses has been observed, when several simple and restricted trails such as Lenz 1950, Liebmann and Grand 1951, Liebmann 1953, and Heath 1966 have been published [2]. Actually, Munro, in 1973, launched the first serious computer-aided investigation into electron lenses [3]. In 1984, Lencová introduced software similar to that of Munro to deal with additional features of a relatively wide analyzed area for magnetic lenses. A numerous of software and simulation programs in electron optics have been presented such as; SOFEM [4], PBO Lab [5], SPOC programs [6], Beam Optics Analysis (BOA) [7], SIMION-7 version [8], MULTIMAG program [9], Electron Optical Design "EOD" [10], Charged Particle Optics "CPO" programs [11], "Focus" software [12], SIMION-8 version [13], "MEBS" software [14], OmniTrak software [15], and ANSYS software [16].

1.2 Optimization

The basic goal of the optimization technique in the field of electron and ion optical systems is to produce electrodes or pole-pieces systems that provide focusing properties with minimum aberrations. That is, the approach aims to improve the quality of the electron device in general and any desirable procedure that leads to the optimum design of an optical electron system. There are two very different optimization methods in the context of electron and ion optics which are analysis and synthesis [17].

Synthesis optimization procedure can be defined as two-step mathematical processes: the first involves optimizing a certain target function (i.e. axial field, axial potential, trajectory of charged particle beams) for specific operational conditions. Whereas, the second step aims to rebuild a lens system that can achieve the optimized target function that was achieved in the first phase [18]. Subsequently spherical aberration which results from objective properties is used to determine the optimum conditions of Scherzer imaging and other parameters in the electron magnetic lenses.

2. Math Concepts

2.1 Mathematical Field Models

Once the synthesis procedure is adopted for executing the optimization procedure, the objective (or target) function should be defined first. However, in the current paper the target function is mainly concerned with approximating the axial flux density (B_z) by a well-known mathematical model. Sixteen different forms were considered (see Table 1), from which the axial magnetic field could be determined and so initiate the synthesis procedure.

Table 1- The Expressions of Mathematical Field Models [19]

Model No.	Model Name	Model Math Form
1	Glaser Bell-Shaped	$B_z=B_{max} / [1+(z / a)^2]$
2	Grivet-Lenz	$B_z=B_{max} / [\cosh(1.317\ z / a)]$
3	Exponential Field	$B_z=B_{max} \exp(-z \ln 2 / a)$
4	Spherical Pole-Piece	$B_z=B_{max} (3.847)^3 / [3.847+(z / a)]^3$
5	Gaussian Field	$B_z=B_{max} \exp[-(z / a)^2 \ln 2]$
6	Fourth Exponent	$B_z=B_{max} / [1+(z / a)^4]$

7	Three Halves Exponent	$B_z=B_{max} / [1+(z / a)^{3/2}]$
8	Inverse Hyperbolic Sine Function	$B_z=B_{max} / \sqrt{1 + (2\sqrt{3}\ z / a)^2}$
9	Inverse Tangent Function	$B_z=B_{max} / [1+(2z / a)^2]$
10	Hyperbolic Tangent	$B_z=B_{max} [1-\{\tanh(1.76275(z / a)\}^2]$
11	Mixed	$B_z=B_{max} \tan^{-1}(z / a) / \sinh(z / a)$
12	Trigonometric function	$B_z=B_{max} / [\{\cosh(z / a)\}^2 \sqrt{2 + \tanh(z / a)}\ ]$
13	Quadratic Secantsh	$B_z=B_{max} [\mathrm{sech}(1.135\ z / a)]^2$
14	Powered Hyperbolic Secantsh	$B_z=B_{max} [\mathrm{sech}(180\ z / (z_2-z_1))]^N$
15	Cosine Field	$B_z=B_{max} [\cos\{z\ (\cos^{-1}(0.5))^{1/N} / W\}]^N$
16	HSH	$B_z = B_{max} . r^4 / (Z^2 + r^2)^2$

2.2 Math Relations and Scherzer Optimum Conditions

2.2.1 The Coefficient of Spherical Aberration and Wavelength

The spherical aberration is a blurring phenomenon that occurs if a lens can not converge incoming rays, those of high incidence angles, to the focal point but directs them to a point that is closer to the lens. This will spread an image point in the image plane (ideally pictured as a single point in the gaussian image plane) over a finite size disc.

For an objective lens, only the spherical and chromatic aberrations are important, since the combined effects of electron wavelength and spherical aberration set the electron-optical resolution limit. While radial and spiral distortions are the most important for intermediate and projector lenses since they cause an image point shift with no blurring [20].

The spherical aberration can be calculated from the integral formula below [20]**:**

$$C_s = \frac{\eta}{128 V_r} \int_{z_o}^{z_i} \left[\frac{3\eta}{V_r} B_z^4 r_\alpha^4 + 8 B_z'^2 r_\alpha^4 - 8 B_z^2 r_\alpha^2 r_\alpha'^2 \right] dz \quad \textbf{(1)}$$

The wavelength (λ in nm) of electron beam is related to its speed (v), which is set by the accelerating voltage (V in volts) in the form [21]:

$$\boldsymbol{\lambda\ (nm) = h / m.v = [(h^2 / 2\ e.m) / V]^{1/2} = (1.5 / V)^{1/2} = 1.23 \times 10^{-6}\ V^{1/2}} \quad \textbf{(2)}$$

Where h is Planks constant and is equal 6.63×10^{-34} J.s, e and m are the charge and the mass of electron , respectively.

2.2.2 Resolution and Resolving Power

Lord Rayleigh, in 1874, developed the most widely used concept of resolution. He proposed a resolution criterion required for the use of a telescope to discriminate between two stars. Thus, this example

is being used to explain the resolution principle but the findings usually apply to other forms of imaging tools such as cameras and microscopes.

Rayleigh principle states; "The midway brightness between the two points is 0.81 of the brightness at the points they are themselves. We can find that to be around the limit of closeness at which some definite indication of resolution may be present".

The point resolution or resolution limit (δ) is defined by the smallest distance (closest spacing) at which two points can be resolved or can clearly be seen through the microscope to be two separate entities [21].

Scherzer's optimum resolution limit in optimum conditions for coherent and incoherent imaging circumstances is given by [22]:

$$\boldsymbol{\delta_{ORLCSI} = 0.667\ (C_S\ \lambda^3)^{1/4}} \quad \text{for coherent imaging} \quad \textbf{(3)}$$

$$\boldsymbol{\delta_{ORLICSI} = 0.61\ (C_s \lambda^3)^{1/4}} \quad \text{in TEM for incoherent imaging} \quad \textbf{(4)}$$

$$\boldsymbol{\delta_{ORLICSI} = 0.43\ (C_s \lambda^3)^{1/4}} \quad \text{in STEM for incoherent imaging} \quad \textbf{(5)}$$

It should be noted that, for incoherent imaging, the Scherzer resolution condition (Eq.5) is significantly higher than that for coherent imaging (Eq. 3) [23]. While the resolving power (γ) (in nm-1) is the inverse of resolution limit, and so the last three equations can be formed as:

$$\gamma_{ORLCSI} = 1.499\ (C_S\ \lambda^3)^{-1/4} \quad \text{for coherent imaging} \quad (6)$$
$$\gamma_{ORLICSI} = 1.639\ (C_s\ \lambda^3)^{-1/4} \quad \text{in TEM for incoherent imaging} \quad (7)$$
$$\gamma_{ORLICSI} = 2.325\ (C_s\ \lambda^3)^{-1/4} \quad \text{in STEM for incoherent imaging} \quad (8)$$

It must noted that, for incoherent imaging, the Scherzer resolution power (resolution condition) is significantly higher than that for coherent imaging [23]. Thus, Scherzer resolution power (Scherzer cutoff frequency or spatial frequency) (γ_{Sch}) is the highest transferred frequency [23], [24]:

$$\gamma_{Sch} = [6 / (C_s\ \lambda^3)]^{1/4} = 1.565\ (C_s\ \lambda^3)^{-1/4} \quad (9)$$

The minimum value of Scherzer resolution power $(\gamma_{Sch})_{min}$ is:

$$(\gamma_{Sch})_{min} = 0.385\ (C_s\ \lambda^3)^{-1/4} \quad (10)$$

2.2.3 Optimum Aperture

The optimum angular, semi–angle aperture, in Scherzer imaging is given by [22]:

$$\alpha_{oSch}\ (rad) = 1.51\ (\lambda / C_S)^{1/4} \quad \text{for coherent imaging} \quad (11)$$
$$\alpha_{oSch}\ (rad) = 1.41\ (\lambda / C_S)^{1/4} \quad \text{for incoherent imaging} \quad (12)$$

Where α is the semi-angle of cones of rays leaving the object point. So, the optimum aperture gives the minimum spot size.

The aperture can be formed in other cases:

$$\alpha_{Hawk}\ (rad) = 0.77\ (\lambda / C_s)^{1/4} \quad \text{up to Hawkes, 1982 [21]} \quad (13)$$
$$\alpha_{Klem}\ (rad) = (\lambda / C_s)^{1/4} = 0.006/(C_s^{1/4}\ V^{1/8}) \quad \text{up to Klemperer, 1971 [25]} \quad (14)$$

2.2.4 Optimum Scherzer Defocus

It is estimated that the deviation of a defocused ray from the ideal is by stating the longitudinal aberration, a measure of how much a ray deviates from the focal point along the optical axis, as opposed to the spherical aberration. . The defocus value (Ψ) can be used to counteract the spherical aberration in order to allow a greater contrast in the process. Scherzer developed this analysis, and is called Scherzer defocus (Ψ_{Sch}) andis formed as [26]:

$$\Psi_{Sch} = (C_s\ \lambda)^{1/2} \quad (15)$$

In the Scherzer defocus, the optimal image condition in bright field mode occurs [27].

Otto Scherzer, in 1949, found that the optimum defocus depends on the microscope properties provided by the electrons, such as the spherical aberration coefficient (Cs), and the electron wavelength (λ) or accelerating voltage (V_r), and is given by:

$$\Psi_{OSch} = -1.2\ (C_s\ \lambda)^{1/2} \quad (16)$$

Where the Scherzer defocus extension is defined by factor 1.2. In general, it is the best defocus for taking images from HRTEM (High Resolution TEM) [28].

Thus, the extended Scherzer defocus is:

$$\Psi_{Sche1} = (1.5\ C_s\ \lambda)^{1/2} = 1.2247\ (C_s\ \lambda)^{1/2} \quad (17)$$

And the extended second broadband Scherzer defocus is:

$$\Psi_{Sche2} = (3.5\ C_s\ \lambda)^{1/2} = 1.87\ (C_s\ \lambda)^{1/2} \quad (18)$$

The second of these, is widely used to describe different image resolution scales.

Additionally, Pennycook and Nellist, in 1997, introduced the optimum conditions for coherent, and incoherent Scherzer imaging circumstances as follows [22]:

$$\Psi_{OSchc} = -1.15(C_s\ \lambda)^{1/2} \quad \text{coherent imaging} \quad (19)$$
$$\Psi_{OSchi} = -(C_s\ \lambda)^{1/2} \quad \text{incoherent imaging} \quad (20)$$

2.2.5 Scherzer Contrast

Mathematically, the contrast transfer function (CTF) explains how aberrations in a transmission electron microscope (TEM) changes a sample image [29], [30]. This CTF sets the resolution of HRTEM, also known as phase contrast of TEM.

The contrast in HRTEM comes from interference between the phases of scattered electron waves with the transmitted electron wave phase in the image plane.

The image would exactly represent the object function in an ideal microscope, and the image intensity for a function of a pure phase object would be equal to 1, that is, the image would show no contrast. This can be compared in an ideal optical microscope with imagery of a glass plate with variable thickness. Thin material objects also behave as phase objects in the transmission electron microscope. In electron microscope , the phase shift for a range of beams can be made approximately equal to $-\pi/2$ if it is operated at optimum focus where a fortunate balance between spherical aberration and defocus is achieved through phase contrast. In addition, the period for a thin object is proportional to the object 's projected potential such that the image contrast can be directly interpreted in terms of the object 's projected structure [24].

Complex interactions occur when an electron wave passes through a sample in TEM. The electron wave above the sample can be approximated as a plane wave.

Owing to spherical aberration and defocus, Scherzer contrast or total phase shift (χ) is:

$$\chi = \pi \Psi \lambda \gamma_{Sch}^2 + 0.5 \pi C_s \lambda^3 \gamma_{Sch}^4 \quad (21)$$

According to the last equation (Eq. 21), it should be noted that the phase shift or Scherzer contrast (χ) depends upon and increases with Scherzer cutoff frequency or resolution power (γ_{Sch}). The process of imaging is also influenced by the effects of spatial and temporal incoherences. Spatial incoherence occurs because the illuminating beam is not parallel but can be considered as a cone of incoherent plane waves (beam convergence). The image, then, results from a superposition of the intensities of the respective images. Temporary incoherence arises from variations in (a) the energy of the thermally released electrons, (b) the lens currents and (c) the accelerating voltage. So, the above effects cause the focus electrons to fluctuate.

5. Results and Discussion Home Page of Optimum Conditions for Scherzer Imaging.

From the home page of the program , model no.1 was selected ,where B_{max} = 0.5 Tesla, z_1 = -10 mm, a_1 = 0.5 mm, a_2 = 0.5 mm (symmetric lens) for Glaser Bell-Shaped Model (GBSM) and using its magnetic flux density (B_z) and zero magnification condition (ZMC) as a case study to compute the optimum conditions for Scherzer imaging (as in Table 2). These parameters were plotted (see Figure 1) to study their behaviors.The outcome results supply the searcher in benefit feedback about the proposed model (lens) from auto use in FILE, EDIT, VIEW, COMPUTE AND PLOT, PATH NAME, and HELP options which are available in the task bar in the home page of this software development according to user need, as shown in Figure 2.

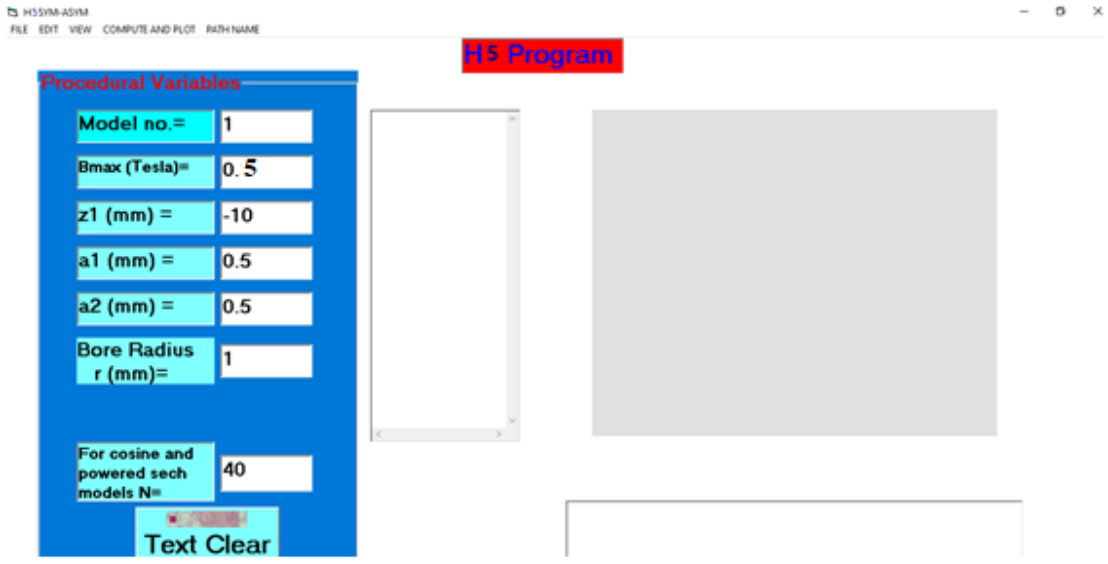

Figure 1-Home Page of Optimum Conditions for Scherzer Imaging.

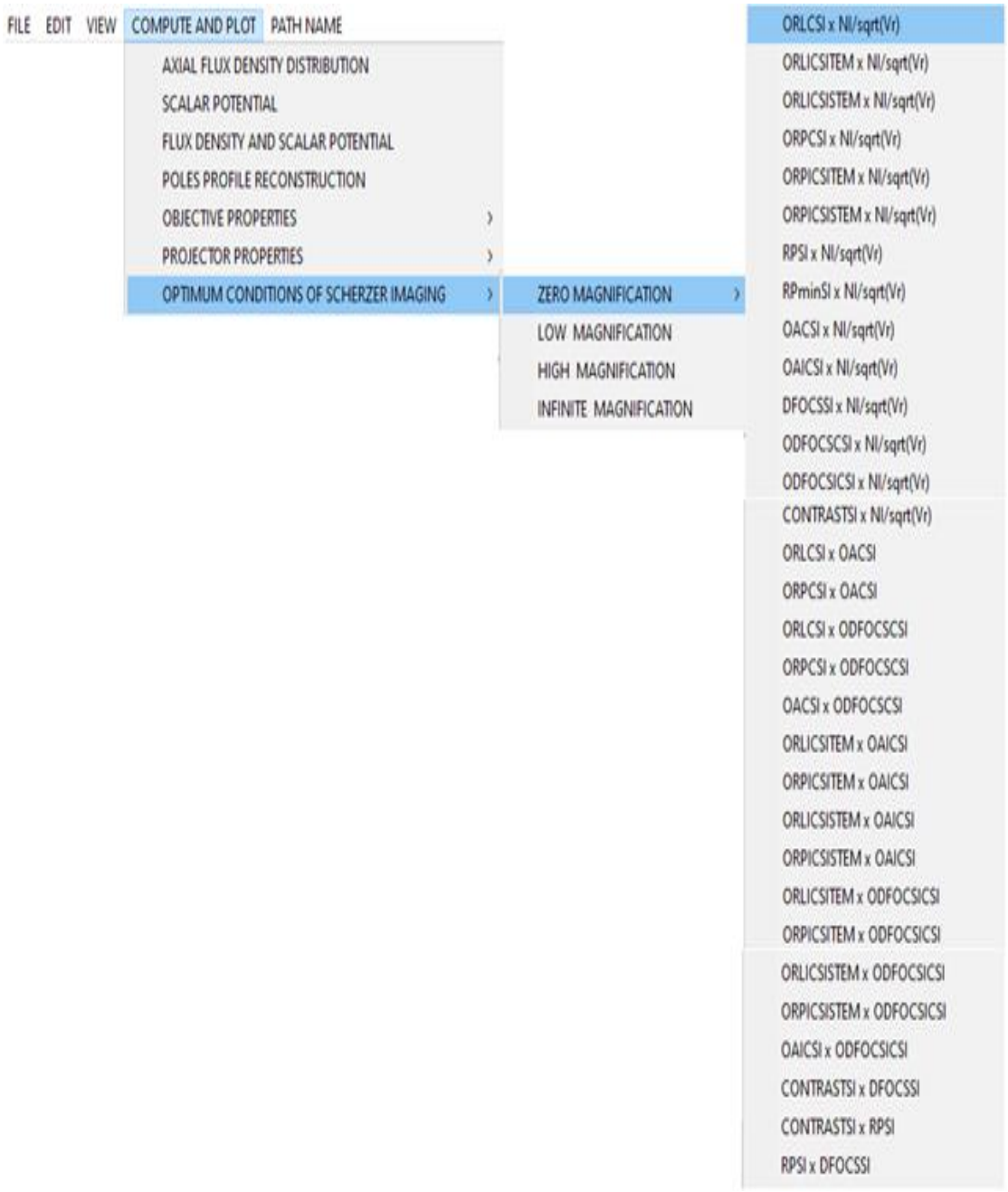

Figure 2-The commands can be excuting as computations and plots at developing of CADTEL software.

Table 2: The optimum conditions for Scherzer imaging of proposed magnetic lens for zero magnification condition

BEAM VOLTAGE	EXCITATION PARAMETER	WAVE LENGTH	SPHERICAL ABERRATION	OPT.RESOLLUM. COHSCHLIMAG.	OPT.RESOLLUM. INCOHSCHLTEM	OPT.RESOLLUM. INCOHSCHLSTEM	OPT.RESOLPOW. COHSCHLIMAG.	OPT.RESOLPOW. INCOHSCHLTEM	OPT.RESOLPOW. INCOHSCHLSTEM	RESOLPOW. SCHLIMAG.	RESOLPOW.MIN. SCHLIMAG.	OPT.APRT. COHSCHLIMAG.	OPT.APRT. INCOHSCHLIMAG.	DEFOCOS SCHLIMAG.	OPT.DEFOCOS COHSCHLIMAG.	OPT.DEFOCOS. INCOHSCHLIMAG.	CONTRAST SCHLIMAG.
Vr(Kv)	NI/sqrt(Vr)	LMDA(nm)	Cs(m)	SGMAOS(nm)	SGMAICSSTEM(nm)	SGMAICSSTEM(nm)	GAMAOS(1/nm)	GAMAICSTEM(1/nm)	GAMAICSSTEM(1/nm)	GAMAS(1/nm)	GAMASmin(1/nm)	ALFAOS(rad)	ALFAIS(rad)	PSIOS(m)	PSIOS(m)	PSIOS(m)	CNTRSTS
366.1727	1	0.00202	618.226651	854.72	781.67	551.02	0.00117	0.0012793	0.0018148	0.0012213	0.0003004	0	0	1.1699354	0.719479	0.6256339	11.0956306
91.54318	2	0.00405	10.03681	111.01	101.52	71.57	0.0090083	0.00985	0.0139733	0.0094033	0.0023133	0	0	0.0379874	0.0233612	0.0203141	42.7153657
40.68586	3	0.00607	0.93883	35.04	32.05	22.59	0.0285348	0.0312012	0.0442621	0.0297862	0.0073276	0.0000000000002	0.0000000000002	0.0053299	0.0032778	0.0028502	90.2045106
22.80579	4	0.0081	0.18241	16.14	14.76	10.41	0.0619579	0.0677474	0.0961068	0.0646751	0.0159105	0.0000000000017	0.0000000000016	0.0013808	0.0008491	0.0007384	146.898686
14.64691	5	0.01012	0.05341	9.23	8.44	5.95	0.1083445	0.1184685	0.16806	0.113096	0.0278223	0.0000000000072	0.0000000000067	0.0005054	0.0003108	0.0002702	205.513561
10.17146	6	0.01214	0.0204	6.09	5.57	3.93	0.1641606	0.1795002	0.2546398	0.1713599	0.0421556	0.0000000000225	0.0000000000021	0.0002316	0.0001424	0.0001239	259.5218346
7.47291	7	0.01417	0.0094	4.46	4.08	2.87	0.2244076	0.2453768	0.3480927	0.234249	0.0576267	0.0000000000569	0.0000000000533	0.0001245	0.0000766	0.0000666	304.1539273
5.72145	8	0.01619	0.00498	3.52	3.22	2.27	0.2838746	0.3104006	0.4403358	0.2963239	0.0728976	0.0000000001228	0.0000000001115	0.0000753	0.0000463	0.0000403	336.7751551
4.52065	9	0.01822	0.00293	2.96	2.7	1.91	0.3381187	0.3697134	0.5244771	0.3529469	0.0868272	0.0000000002343	0.0000000002194	0.00005	0.0000307	0.0000267	356.7193773
3.66173	10	0.02024	0.00188	2.6	2.38	1.68	0.3840131	0.4198963	0.5956669	0.400854	0.0986127	0.0000000004056	0.0000000003798	0.0000356	0.0000219	0.0000191	364.8161903
3.02622	11	0.02226	0.0013	2.38	2.18	1.54	0.4196169	0.458827	0.650894	0.4380191	0.1077555	0.0000000006649	0.0000000006077	0.000027	0.0000166	0.0000144	362.5972682
2.54287	12	0.02429	0.00094	2.25	2.06	1.45	0.4486589	0.4902347	0.6902347	0.4644934	0.1142684	0.0000000009747	0.0000000009127	0.0000214	0.0000131	0.0000114	352.6523936
2.1667	13	0.02631	0.00072	2.17	1.99	1.4	0.4599583	0.502938	0.7134701	0.4801297	0.118115	0.0000000013877	0.0000000012994	0.0000176	0.0000108	0.0000094	336.6315738
1.86823	14	0.02834	0.00057	2.15	1.97	1.39	0.4653884	0.5088755	0.7218932	0.485798	0.1195094	0.0000000018885	0.0000000017685	0.0000015	0.0000092	0.000008	316.381592
1.62743	15	0.03036	0.00047	2.17	1.99	1.4	0.460186	0.5031187	0.7138235	0.4803675	0.1181735	0.0000000024609	0.0000000023044	0.0000132	0.0000081	0.0000071	292.0381023
1.43036	16	0.03238	0.0004	2.27	2.08	1.47	0.4397621	0.4807003	0.6819237	0.4589006	0.1128925	0.0000000030433	0.0000000028499	0.0000122	0.0000075	0.0000065	261.5247377
1.26703	17	0.03441	0.00034	2.28	2.09	1.47	0.4384025	0.479368	0.6800337	0.4576287	0.1125796	0.0000000038678	0.0000000036219	0.0000108	0.0000066	0.0000058	245.509207
1.13016	18	0.03643	0.00031	2.51	2.29	1.62	0.3987781	0.436041	0.6185698	0.4162665	0.1024042	0.0000000044422	0.0000000041408	0.0000106	0.0000065	0.0000057	210.8122519
1.01433	19	0.03846	0.00027	2.53	2.31	1.63	0.3955925	0.4325577	0.6136284	0.4129413	0.1015862	0.0000000054457	0.0000000050995	0.0000096	0.0000059	0.0000051	198.1472898
0.91543	20	0.04048	0.00024	2.61	2.39	1.68	0.3832724	0.4190864	0.5945179	0.4000808	0.0984224	0.0000000064777	0.0000000060659	0.0000089	0.0000055	0.0000048	182.3690745

THE ABOVE RESULTS ARE FOR AN EXCITATION OF NI = 605.12 AMPTURNS

According to the above equations , the programing code for all proposed math models of lenses was written, to compute and plot the optimum conditions for Scherzer imaging.

At ZMC for a magnetic lens using GBSM and as a function of excitation parameter ($NI/\sqrt{Vr}$), Figures 3-16 illustrate the optimum resolution limit (δ) for coherent Scherzer imaging, the optimum resolution limit (δ) for coherent Scherzer imaging in TEM, the optimum resolution limit (δ) for incoherent Scherzer imaging in STEM, the optimum resolution power (γ) for coherent Scherzer imaging, the optimum resolution power (γ) for incoherent Scherzer imaging in TEM, the optimum resolution power (γ) for incoherent Scherzer imaging in STEM, the resolution power (γ) for Scherzer imaging, the minimum resolution power (γ_{min}) for Scherzer imaging, the optimum aperture (α) for coherent Scherzer imaging, the optimum aperture (α) for incoherent Scherzer imaging, the defocus (ψ) for Scherzer imaging, the optimum defocus (ψ) for coherent Scherzer, the optimum defocus (ψ) for incoherent Scherzer imaging, and the contrast (χ) for Scherzer imaging.

The user can evaluate and observe the relations of the optimum resolution limit (δ) and the optimum resolution power (γ) as a function of optimum aperture (α) as shown in Figures 17 and 18, and as a function of optimum defocus (ψ) as illustrated in Figures 19and 20 respectively, for coherent Scherzer imaging at ZMC for magnetic lens using GBSM.

The development of CADTEL software provides the user the capability to study the effect of other parameters such as, the optimum aperture (α) as a function of optimum defocus (ψ) for coherent Scherzer imaging (Figure 21). In addition, as a function of optimum aperture (α), when the user can examine the optimum resolution limit (δ) in TEM, the optimum resolution power (γ) in TEM, the optimum resolution limit (δ) in STEM, and the optimum resolution power (γ) in STEM, as illustrated in Figures 22, 23, 24, and 25, respectively for incoherent Scherzer imaging at ZMC for magnetic lens using GBSM.

Thus, user can study the variation of numerous parameters such as the optimum resolution limit (δ) in TEM, the optimum resolution power (γ) in TEM, the optimum resolution limit (δ) in STEM, the optimum resolution power (γ) in STEM, the optimum aperture (α), and the contrast (χ) as a function of optimum defocus (ψ) as shown in Figures 26, 27, 28, 29, 30, and 31, respectively, for incoherent Scherzer imaging at ZMC using GBSM.

Finally, Figures 32 and 33 represent the relation between the contrast (χ) as a function of resolution power (γ), and the behavior of the resolution power (γ) as a function of defocus (ψ), respectively for Scherzer imaging at ZMC using GBSM.

6. Conclusions

In magnetic lenses, according to proposed mathematical model, which is selected from multi-choices in the developed version of CADTEL software, using GBSM at ZMC, studying the optimum desirable design and observing the optimum conditions of coherent and incoherent Scherzer imaging, one can conclude:

- ❖ Optimum resolution limit for coherent and incoherent of TEM and STEM decreases exponentially with increasing the excitation parameters and the optimum aperture values.
- ❖ Increasing the resolving power and its optimum values is associated with the increase of the excitation parameters up to $NI/\sqrt{Vr} = 14$ and decreasing above this value..
- ❖ Exponential increment of the optimum aperture for coherent and incoherent Scherzer imaging occurs with increasing the excitation parameters.
- ❖ Defocus and its optimum values for coherent and incoherent Scherzer imaging exponentially decreases with decreasing the excitation parameters.
- ❖ Contrast rises with incrementing the excitation parameter up to $NI/\sqrt{Vr} =10$, then going down after this value.
- ❖ The optimum resolution power increases with increasing the optimum aperture and declining with the optimum defocus reaching to $\gamma = 0.465$ nm^{-1} for coherent Scherzer imaging, $\gamma = 0.508$ nm^{-1} in TEM for incoherent Scherzer imaging, and $\gamma = 0.721$ nm^{-1} in STEM for incoherent Scherzer imaging, then drops with the increase of optimum aperture and optimum defocus values.

❖ There is a general behavior of increase of the optimum resolution limit with raising the optimum defocus for coherent and incoherent Scherzer imaging of TEM and STEM.
❖ Thus, the optimum aperture decreases with the decrease of the optimum defocus in coherent and incoherent Scherzer imaging.
❖ Also, the contrast increases with the decrease of the defocus up to $\chi = 364$ at $\psi = 0.000035$ m, after these values the contrast decreases with the decrease of defocus Scherzer imaging.
❖ Therefore, the contrast increases with incrementing the resolution power up to $\chi = 364$ at $\gamma = 0.4$ nm^{-1}, then dropping with the decrease of these values of resolution power.
The CADTEL software package is an important new tool for the design and analysis of electro-magnetic lenses. This software provides an interactive and intuitive programming package for the creation of symmetric and asymmetric lenses for one or more pole piece in both the analysis and synthesis process under four operating conditions. CADTEL provides a substantial decrease in time, and effort needed to inform a beginner user interested in this field. Therefore, the increased performance should be realized because from the field of electron optics.

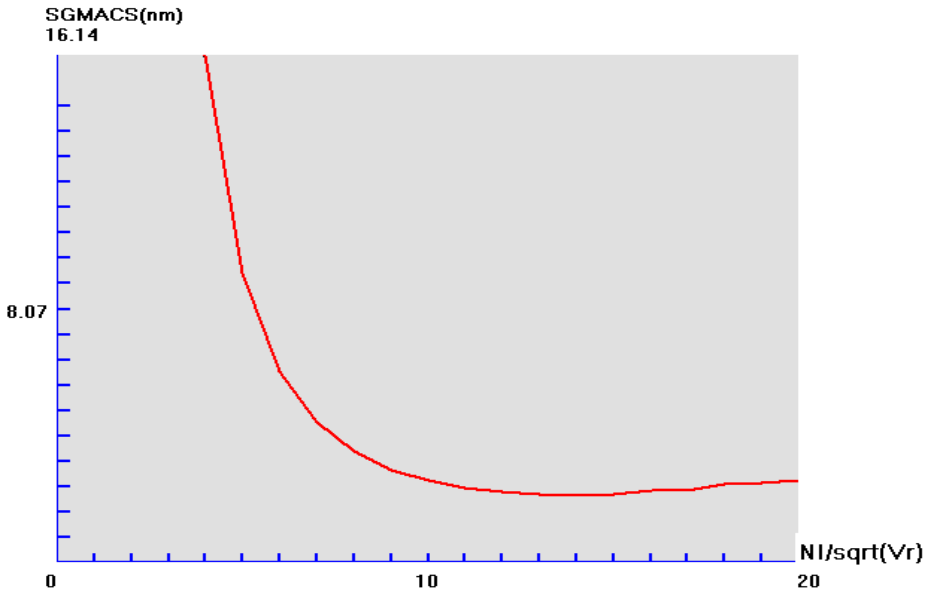

Figure 3- The optimum resolution limit (δ) for coherent Scherzer imaging as a function NI/√Vr at ZMC for magnetic lens using GBSM.

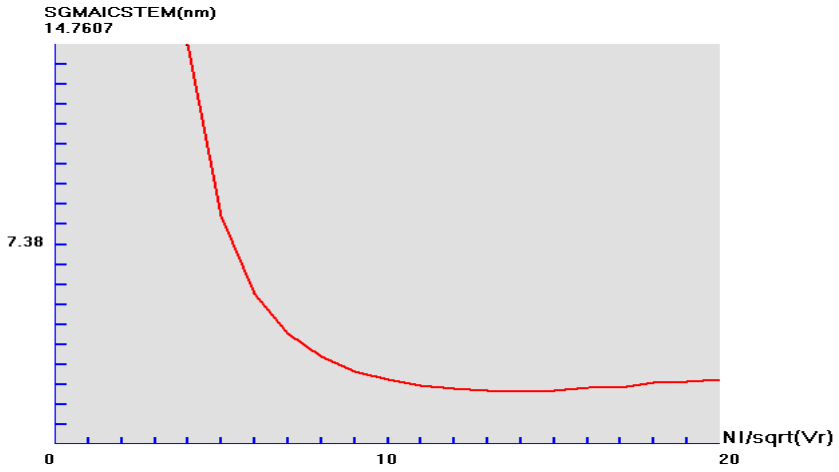

Figure 4-The optimum resolution limit (δ) for coherent Scherzer imaging in TEM as a function of NI/√Vr at ZMC for magnetic lens using GBSM.

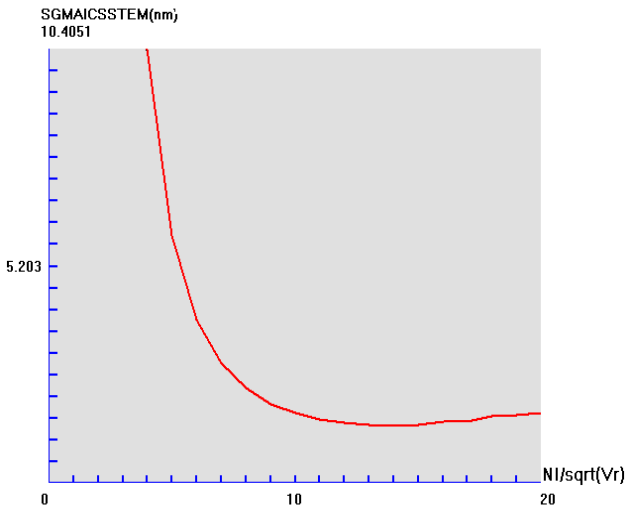

Figure 5- The optimum resolution limit (δ) for incoherent Scherzer imaging in STEM as a function of NI/√Vr at ZMC for magnetic lens using GBSM.

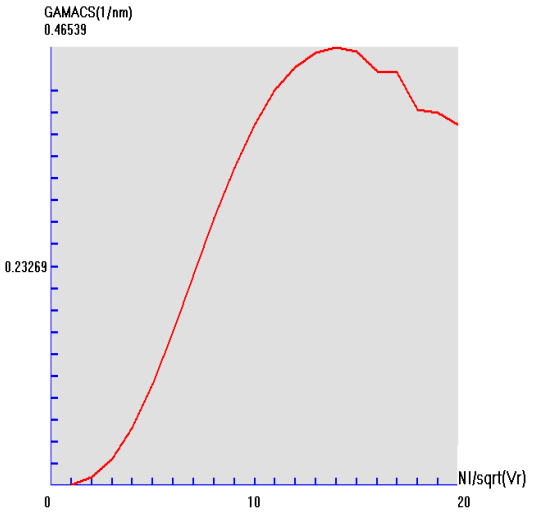

Figure 6- The optimum resolution power (γ) for coherent Scherzer imaging as a function of NI/√Vr at ZMC for magnetic lens using GBSM.

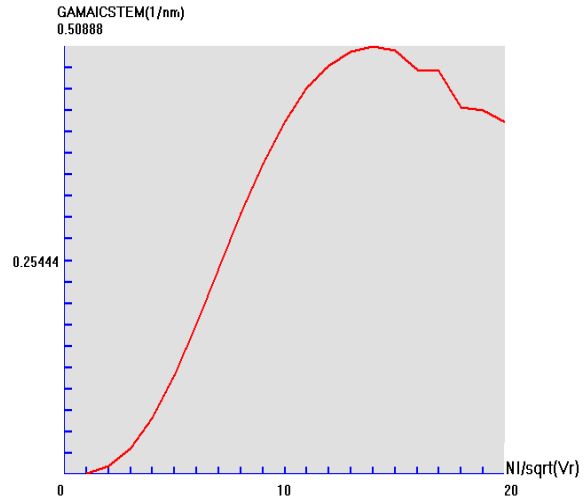

Figure 7: The optimum resolution power (γ) for incoherent Scherzer imaging in TEM as a function of NI/√Vr at ZMC for magnetic lens using GBSM.

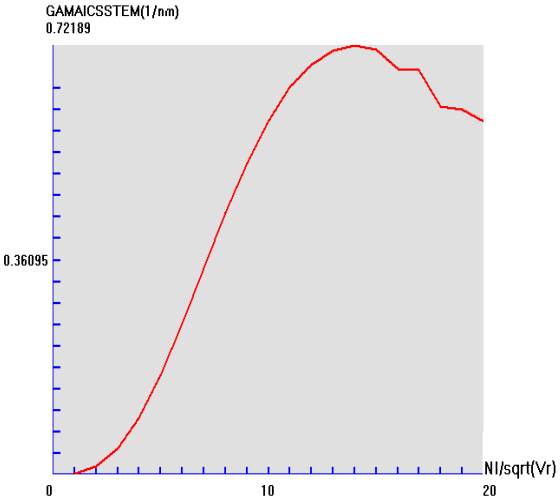

Figure 8: The optimum resolution power (γ) for incoherent Scherzer imaging in STEM as a function of NI/√Vr at ZMC for magnetic lens using

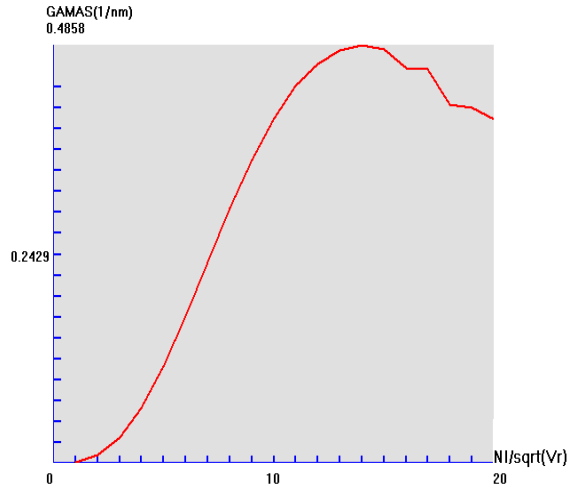

Figure 9- The resolution power (γ) for Scherzer imaging as a function of NI/√Vr at ZMC for magnetic lens using GBSM.

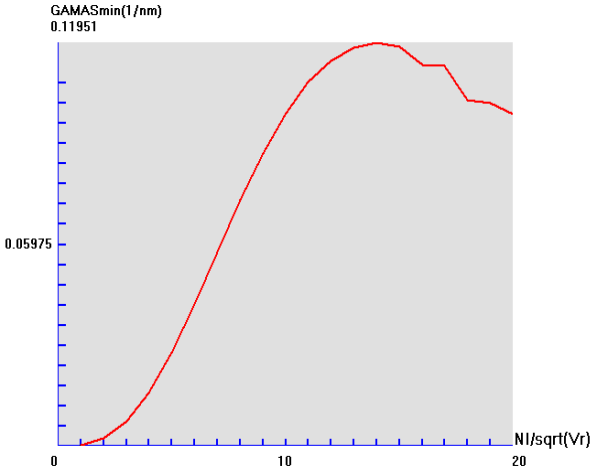

Figure 10- The minimum resolution power (γ_{min}) for Scherzer imaging as a function of NI/√Vr at ZMC for magnetic lens using GBSM.

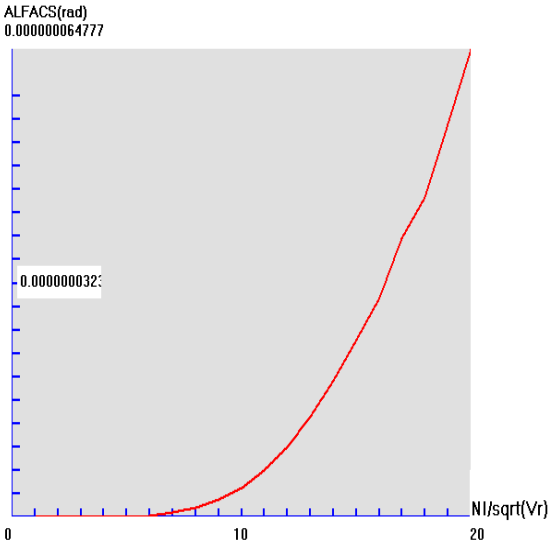

Figure 11- The optimum aperture (α) for coherent Scherzer imaging as a function of NI/√Vr at ZMC for magnetic lens using GBSM.

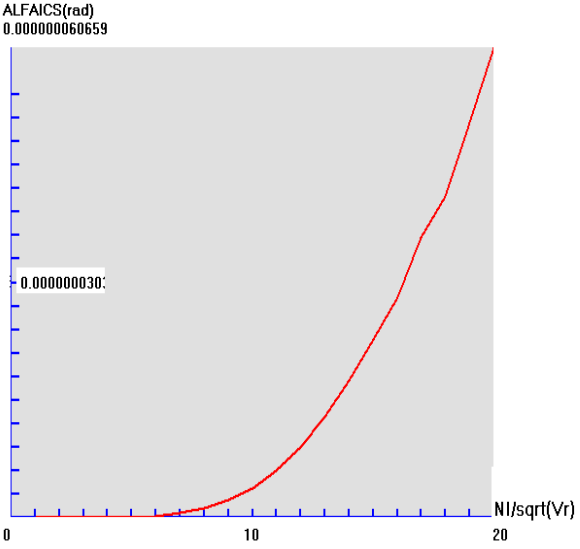

Figure 12- The optimum aperture (α) for incoherent Scherzer imaging as a function of NI/√Vr at ZMC for magnetic lens using GBSM.

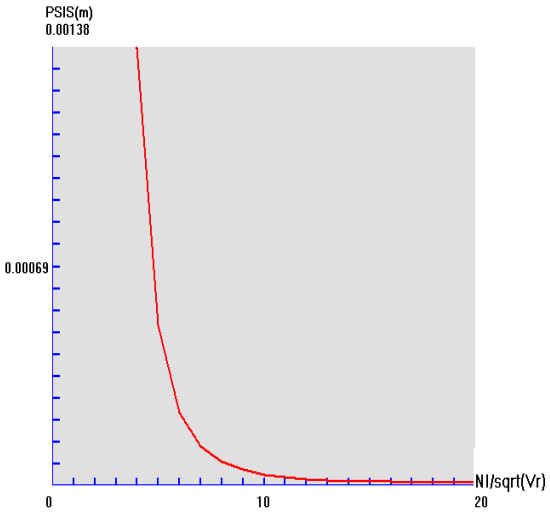

Figure 13- The defocus (ψ) for Scherzer imaging as a function of NI/√Vr at ZMC for magnetic lens using GBSM.

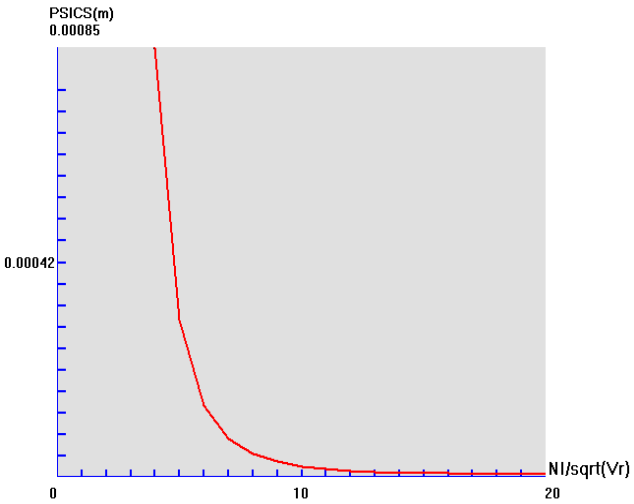

Figure 14-The optimum defocus (ψ) for coherent Scherzer imaging as a function of NI/√Vr at ZMC for magnetic lens using GBSM.

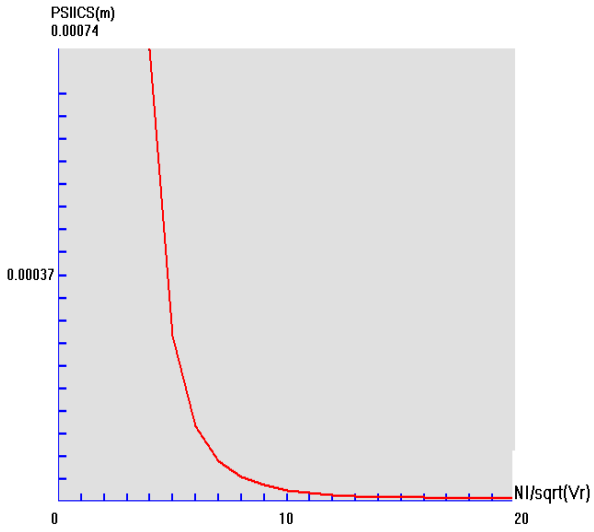

Figure 15-The optimum defocus (ψ) for incoherent Scherzer imaging as a function of NI/√Vr at ZMC for magnetic lens using GBSM.

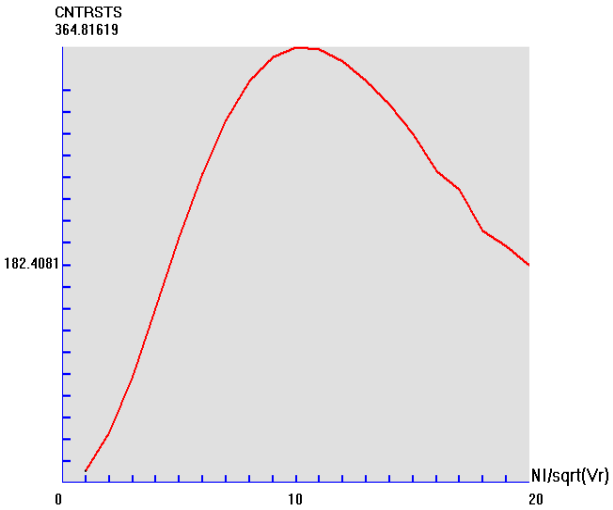

Figure 16- The contrast (χ) for Scherzer imaging as a function NI/√Vr at ZMC for magnetic lens using GBSM.

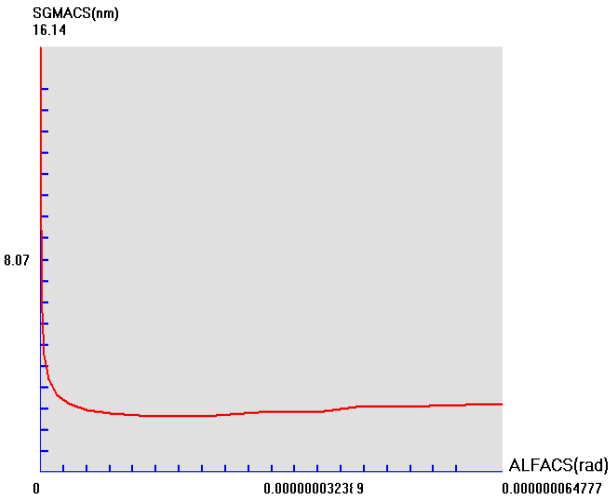

Figure 17-The optimum resolution limit (δ) as a function of optimum aperture (α) for coherent Scherzer imaging at ZMC for magnetic lens using GBSM.

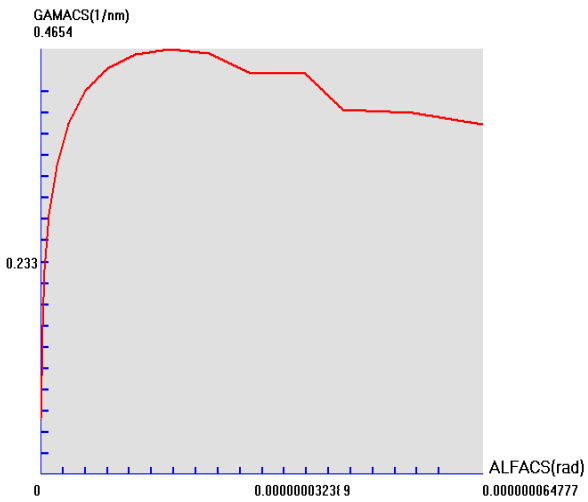

Figure 18- The optimum resolution power (γ) as a function of optimum aperture (α) for coherent Scherzer imaging at ZMC for magnetic lens using GBSM.

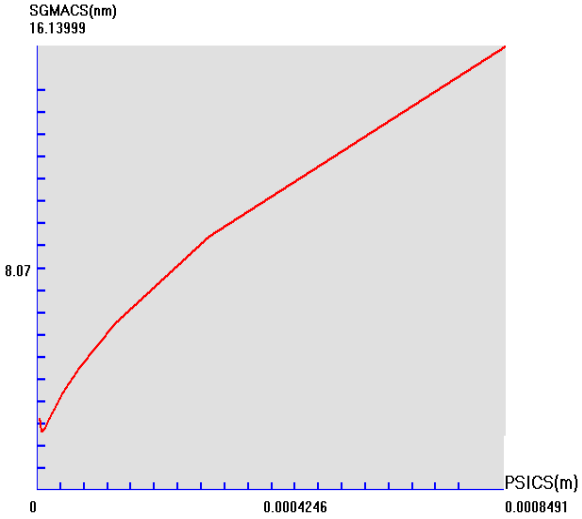

Figure 19- The optimum resolution limit (δ) as a function of optimum defocus (ψ) for coherent Scherzer imaging at ZMC for magnetic lens using GBSM.

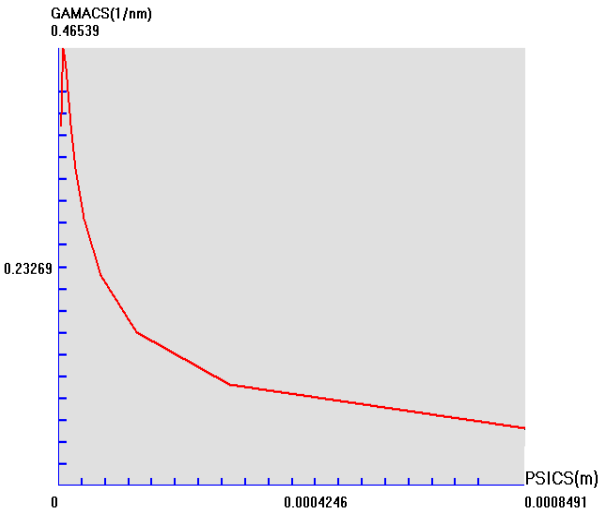

Figure 20- The optimum resolution power (γ) as a function of optimum defocus (ψ) for coherent Scherzer imaging at ZMC for magnetic lens using GBSM.

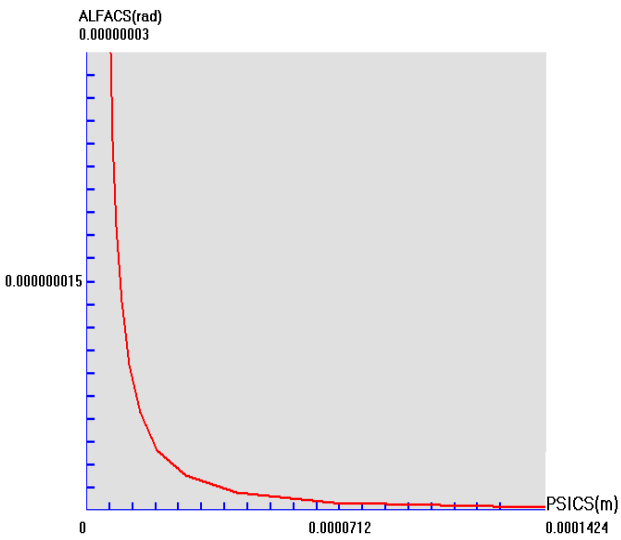

Figure 21- The optimum aperture (α) as a function of optimum defocus (ψ) for coherent Scherzer imaging at ZMC for magnetic lens using GBSM.

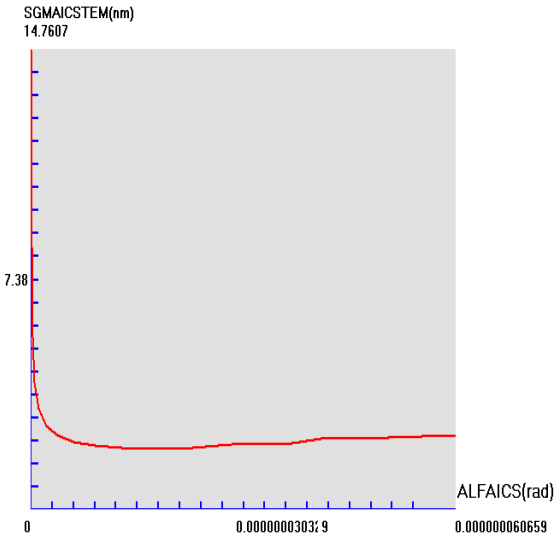

Figure 22- The optimum resolution limit (δ) as a function of optimum aperture (α) for incoherent Scherzer imaging in TEM at ZMC for magnetic lens using GBSM.

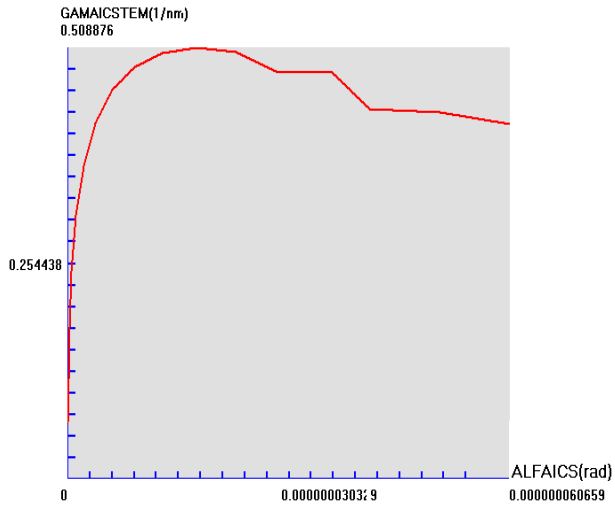

Figure 23- The optimum resolution power (γ) as a function of optimum aperture (α) for incoherent Scherzer imaging in TEM at ZMC for magnetic lens using GBSM.

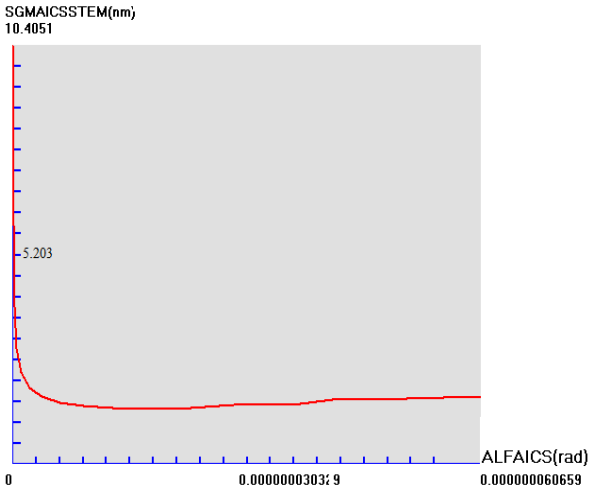

Figure 24-The optimum resolution limit (δ) as a function of optimum aperture (α) for incoherent Scherzer imaging in STEM at ZMC for magnetic lens using GBSM.

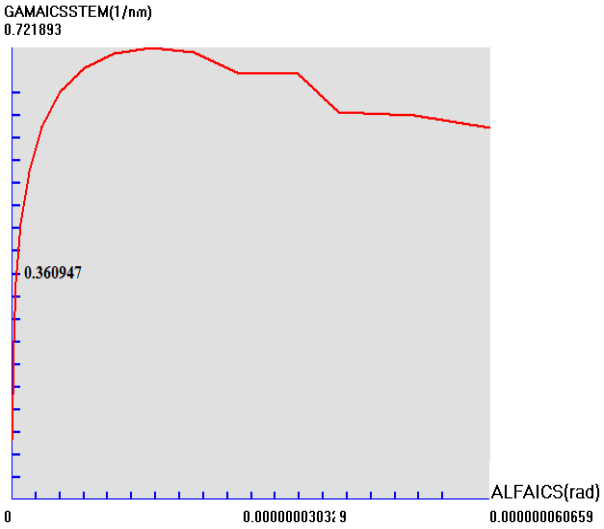

Figure 25- The optimum resolution power (γ) as a function of optimum aperture (α) for incoherent Scherzer imaging in STEM at ZMC for magnetic lens using GBSM.

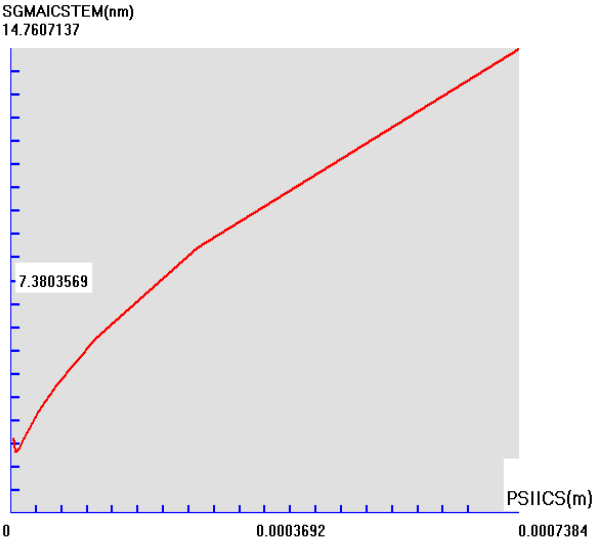

Figure 26- The optimum resolution limit (δ) as a function of optimum defocus (ψ) for incoherent Scherzer imaging in TEM at ZMC for magnetic lens using GBSM.

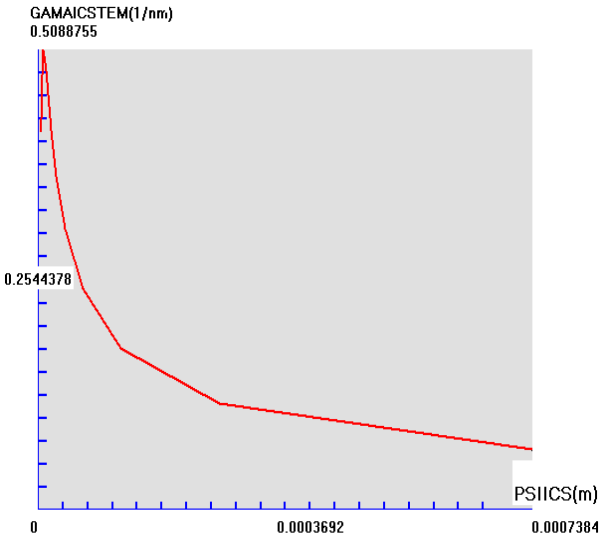

Figure 27-The optimum resolution power (γ) as a function of optimum defocus (ψ) for incoherent Scherzer imaging in TEM at ZMC for magnetic lens using GBSM.

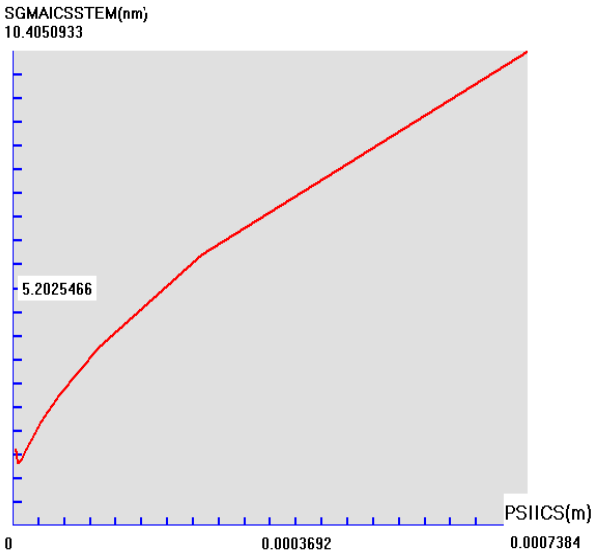

Figure 28- The optimum resolution limit (δ) as a function of optimum defocus (ψ) for incoherent Scherzer imaging in STEM at ZMC for magnetic lens using GBSM.

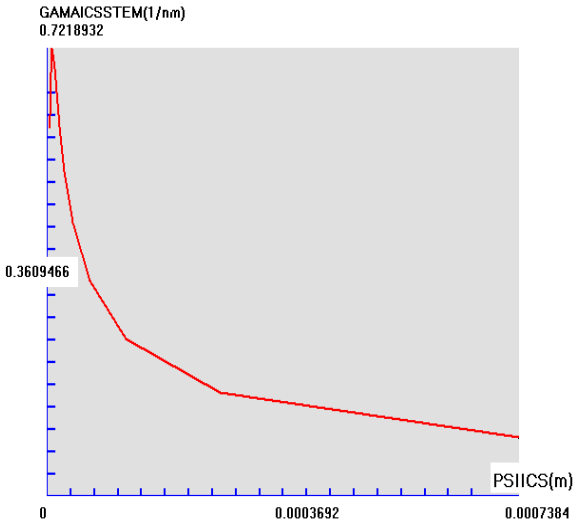

Figure 29-The optimum resolution power (γ) as a function of optimum defocus (ψ) for incoherent Scherzer imaging in STEM at ZMC for magnetic lens using GBSM.

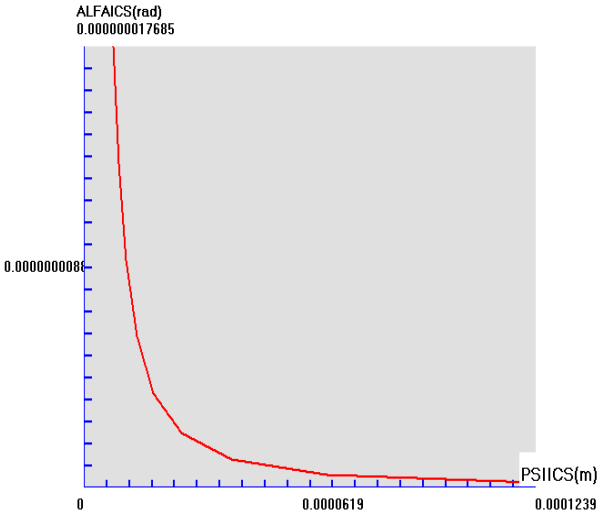

Figure 30- The optimum aperture (α) as a function of optimum defocus (ψ) for incoherent Scherzer imaging at ZMC for magnetic lens using GBSM.

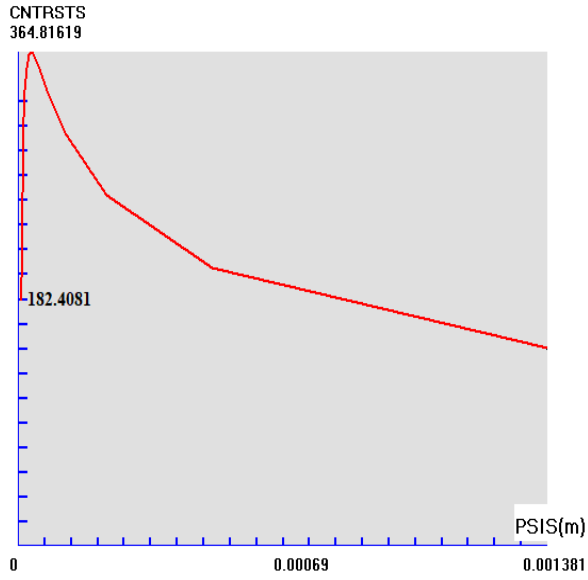

Figure 31- The contrast (χ) as a function of defocus (ψ) for Scherzer imaging at ZMC for magnetic lens using GBSM.

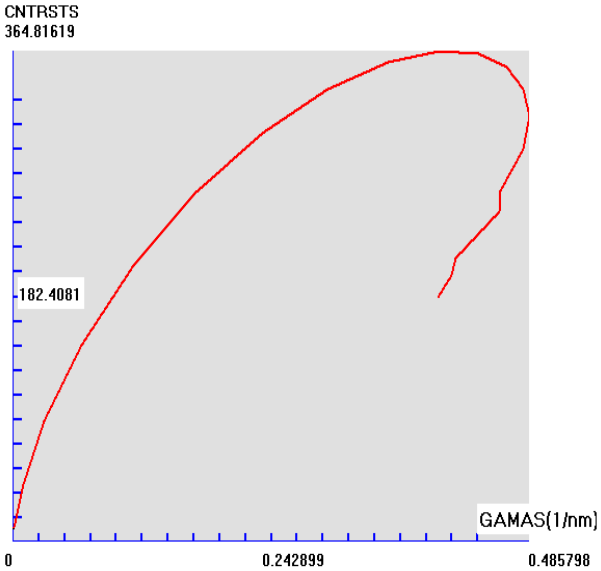

Figure 32- The contrast (χ) as a function of resolution power (γ) for Scherzer imaging at ZMC for magnetic lens using GBSM.

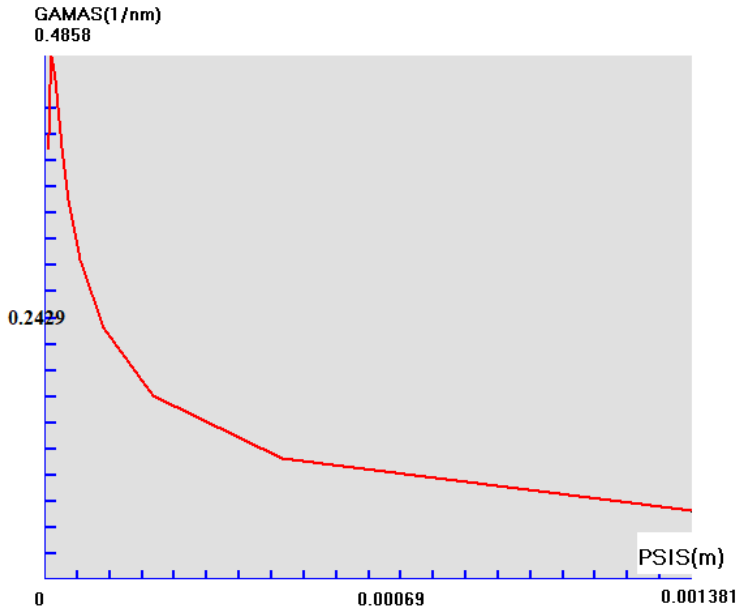

Figure 33- The resolution power (γ) as a function of defocus (ψ) for Scherzer imaging at ZMC for magnetic lens using GBSM.

References

[1] Hasan H. S. "Building a New Software of Electromagnetic Lenses (CADTEL)". *International Letters of Chemistry, Physics and Astronomy*, vol. 9, pp.46-55, 2013.

[2] Munro, E. "*Computer- Aided Design Methods in Electron optics*". Ph.D. Thesis, Univ. of Cambridge, UK, 1971.

[3] Munro, E. *Computer- aided design of electron lenses by the finite element method, in Image Processing and Computer - Aided Design in Electron Optics. Hawkes, P. W. Ed., Academic Press, London*, pp. 284-323, 1973.

[4] Kato, M. and Tsuno, K. "Optimization of Electron Lens Shape Giving Minimum Spherical Aberration Coefficient". *IEEE Transaction on Magnetic*, vol.26, no.2, pp.1023-1025, 1990.

[5] Gillespie, G.H. , Hill, B.W. , Martono, H. Moore J.M. N.A. Brown; M.C. Lampel; R.C. Babcock The Particle Beam Optics Interactive Computer Laboratory for Personal Computers and Workstations. Proceedings of the 1997 Particle Accelerator Conference, vol.2, pp. 2562-2564, 1997 .

[6] Lencová, B. *Software for Particle Optics Computations SPOC*. Fleischnerova 15, 63500 *Brno, Czech Republic*, 2000.

[7] Ives, L., Bui, T., Vogler W. and Cendes Z. "BOA - a Finite Element Charged Particle Code with Adaptive, Finite Element Meshing". *International Vacuum Electronics Conference* , pp. 2, 2000.

[8] Dahl, D. A. "SIMION for personal computer in reflection". *Int. J. Mass Spectrom*. vol.200, no.1-3, pp.3-25, 2000.

[9] Chernosvitov, A., Kalimov, A. and Wollnik, H. "Design of an iron dominated quadrupole magnet with a high pole-tip flux density". *IEEE Trans. Appl. Supercond*., vol.12, no. 1, pp.1430–1433, 2002.

[10] Lencová, B. and Zlámal, J. A new program for the design of electron microscopes. Proceedings of the Seventh International Conference on Charged Particle Optics, Physics Procedia, vol. 1, no. 1, pp.315–324, 2008.

[11] Read F. H. and Bowring N. Nuclear Instruments and Methods in Physics Research Section A: Accelerators Spectrometers Detectors and Associated Equipment. Article in The CPO programs and the BEM for charged particle optics, vol. 645, no.1, pp.273-277, 2011.

[12] Trubitsyn, A. A. "Software FOCUS for axi-symmetrical electron optic systems modeling: Algorithms and Characteristics". *Applied Physics* (Rus.), vol. 2, pp.56-62, 2008.

[13] Manura, D. *SIMION ® 8.0 User Manual*. Scientific Instrument Service (SIS), Inc., issue 172, USA, 2008.
[14] Munro, E. *Munro's Electron Beam Software – Software Catalogue*. MEBS Ltd, 2010.
[15] Humphries, S. *Three-dimensional Charged-particle Optics and Gun Design*. *Field Precision LLC, CRC Press, Albuquerque, New Mexico U.S.A*, 2011.
[16] Holcakova, R. and Marek, M. Innovative research in electron microscopes, analysis of magnetic field distribution of some types of magnetic lenses by FEM. 10th International Conference on Environment and Electrical Engineering , pp.1-4, 2011.
[17] Szilagyi, M. *Electron and Ion Optics*. Plenum Press: New York, 1988.
[18] Al-Jubori, W. J. Inverse Design of Asymmetrical Magnetic Lenses in the Absence of Magnetic Saturation. Ph.D. Thesis, College of Science, University of Al-Mustansiriyah, Baghdad, Iraq, 2001.
[19] Hasan, H.S. A Computer Aided Designing Tools for Electron Lenses A Computer Aided Designing Tools for Electron Lenses. Ph.D. Thesis, the University of Mustansiriyah, Baghdad, Iraq, 2012.
[20] Al-Obaidi, H. N. *Electron Lenses*. *The summer school on Microscopy, Milano, Italy*, 2009.
[21] Goodhew, P. J., Humphreys, J. and Beanland, R. *Electron Microscopy and Analysis*. *Third edition, ISBN*, 2001.
[22] Pennycook, S. J. and Nellist, P. D. *Scanning transmission electron microscopy: Z-contrast*, 1997.
[23] Amenlinckx, S., Dyck, D. van, Landuyt, J. van, and Tendeloo, G. van. *Electron Microscopy Principles and Fundamentals*. VCH 4P A Wiley company, Germany, 1997.
[24] Hawkes, P.W. *Advances in IMAGING and ELECTRON PHYSICS*. Vol.123, *Elsevier Science USA, Academic press: London*, 2002.
[25] Klemperer, O. *Electron Optics*. *Third Edition, Cambridge University Press*, 1971.
[26] Scherzer, O. "The theoretical resolution limit of the electron microscope". *Journal of Applied Physics*, vol..20, no. 1, pp.20–29. Bibcode: 1949JAP....20...20S, 1949.
[27] Reimer, Ludwig, Kohl, and Helmut. *Transmission Electron Microscopy - Physics of Image Formation*. *Springer Series in Optical Sciences*, 2008.
[28] Liao, Y. *Practical Electron Microscopy and Database*, 2007.
[29] Reimer, L. *Transmission electron microscopy: Physics of image formation and microanalysis*. *4th ed., Springer, Berlin preview*, 1997.
[30] Kirkland, E. J. *Advanced computing in electron microscopy*. *Plenum Press, NY*, 1998.